Sensors and Actuators B 204 (2014) 224–230

Contents lists available at ScienceDirect

Sensors and Actuators B: Chemical

journal homepage: www.elsevier.com/locate/snb

Hierarchical flower-like WO_3 nanostructures and their gas sensing properties

Chong Wang, Ruize Sun, Xin Li, Yanfeng Sun*, Peng Sun, Fengmin Liu, Geyu Lu*

State Key Laboratory on Integrated Optoelectronics, College of Electronic Science and Engineering, Jilin University, 2699 Qianjin Street, Changchun 130012, People's Republic of China

ARTICLE INFO

Article history:
Received 18 May 2014
Received in revised form 16 July 2014
Accepted 17 July 2014
Available online 27 July 2014

Keywords:
WO_3
Hierarchical nanostructure
Flower-like
NO_2 sensor

ABSTRACT

Flower-like WO_3 composed of nanosheets were successfully synthesized by calcining the acid-treated hydrothermal precursor. Field emission scanning electron microscopy and transmission electron microscopy results reveal that the flower-like WO_3 are assembled by a number of irregular-shaped nanosheets, which are cross-linked in the interior of the microflower. A possible formation mechanism is proposed on the basis of the results of time-dependent experiments. Moreover, the gas sensing properties of the obtained flower-like nanostructured WO_3 were investigated. It is found that the sensor based on the flower-like WO_3 nanostructure exhibits good selectivity and high response to NO_2, and the detection limit is about 2 ppb.

1. Introduction

In recent years, functional materials have been extensively studied due to their unique physical and chemical properties compared to solid structures [1]. Among them, oxide semiconductor materials occupy an important position. Therefore, much effort has been devoted to the study of various oxide semiconductor materials such as ZnO [2,3], SnO_2 [4,5], CuO [6,7], In_2O_3 [8,9] and TiO_2 [10,11].

Tungsten oxide is a very important n-type ($Eg \approx 3.2$ eV) oxide semiconductor which offers manifold technological applications including lithium ion batteries, photoelectrochemical, solar energy and so on [12–15]. One of the most important applications of WO_3 material is in gas sensors which has been found to show remarkable gas sensing properties for the detection of NO_2 [38–40]. Due to its excellent performance and practical application, a variety of routes have been employed to obtain WO_3 crystal such as thermal evaporation [16], electrochemical precipitation [17] and sol–gel [18]. It is well known that high response and superior selectivity are important parameters in designing semiconductor gas sensors [19]. Therefore, increasing the response and improving the selectivity of oxide semiconductor gas sensors are major scientific challenges for developing new sensor strategies. As many groups have reported before, the morphology plays an important role in determining the properties of materials [20–22]. Hence, various morphologies of WO_3 with different dimensional nanostructures have been synthesized in order to improve the performance of devices based on WO_3, such as nanowire [23], nanoplate [24], hollow-sphere [25], urchin-like [26] and many other hierarchically complex micro/nanostructures [27–30]. However, it is still a challenge to organize the 1D/2D WO_3 nanostructure into well-defined 3D nanostructure in order to obtain high performance NO_2 gas sensor.

In this work, the precursor was synthesized by using $NiCl_2{\cdot}6H_2O$ and $Na_2WO_4{\cdot}2H_2O$ through a hydrothermal method. Then, an acid-treated method and subsequent heat treatment at 500 °C for 2 h were used to prepare the flower-like WO_3. Moreover, the formation process has been investigated through the morphology evolution with different acidification times, and a possible formation mechanism is speculated. The sensors based on the synthesized flower-like WO_3 exhibit a high response to NO_2, and the response of the sensor to 2 ppb NO_2 is about 12.8. To our knowledge, WO_3 with this novel nanostructure with such high sensitivity was first synthesized.

2. Experimental

All the reagents (analytical-grade purity) were used without any further purification.

The precursor was synthesized under hydrothermal condition. In a typical synthesis, 4 mmol $Na_2WO_4{\cdot}2H_2O$ and 0.8 g of sodium dodecyl benzene sulfonate (SDBS) were dissolved in 20 ml distilled water to form a homogeneous solution under vigorous stirring.

* Corresponding authors. Fax: +86 431 85167808.
E-mail addresses: syf@jlu.edu.cn (Y. Sun), lugy@jlu.edu.cn (G. Lu).

http://dx.doi.org/10.1016/j.snb.2014.07.083
0925-4005/

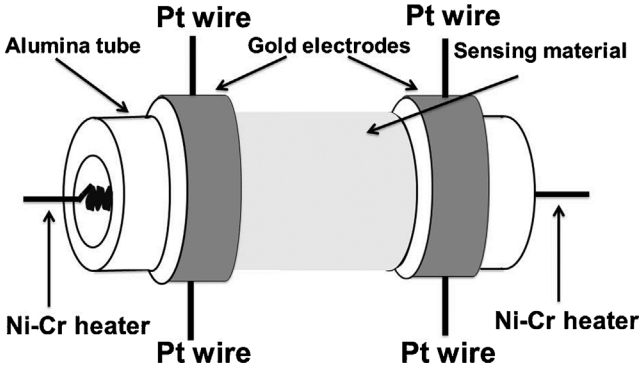

Fig. 1. Schematic structure of the gas sensor.

Then 20 ml aqueous $NiCl_2$ solution (0.2 M) was added into the above solution. Ten minutes later, the mixture solution was transferred into a Teflon-lined stainless steel autoclave, sealed tightly, and maintained at 160 °C for 24 h. After the autoclave was cooled to room temperature naturally, the green product was collected by washing with deionized water and absolute ethanol for several times, and dried at 80 °C for 1 day.

To get the flower-like WO_3 sample, the acidification experiment was then performed. The green precursor was immersed in 4 M HNO_3 and maintained at room temperature for 21 h statically. During this process, the color of the solution was changed gradually from green to yellow. The yellow product was then washed with deionized water and absolute ethanol for several times and dried at 80 °C in air. Finally, the acid-treated product was calcined at 500 °C to get the WO_3 sample.

A sensor device was fabricated using the obtained WO_3 powder. Firstly, a suitable amount of WO_3 powder was mixed with ethanol to obtain a paste which was then coated onto an alumina tube (4 mm in length, 1.2 mm in external diameter and 0.8 mm in internal diameter) using a small brush slowly and lightly. The tube was installed with a pair of gold electrodes, and each electrode was connected with two Pt wires. After drying in air for a while, the thin film with proper thickness was formed. Then the tube was placed in a muffle furnace and the temperature was kept at 300 °C for 2 h. When the temperature was reduced to room temperature, the tube with sensing film was soldered to the pedestal. Finally, a Ni–Cr alloy coil was inserted into the alumina tube as a heater in order to control the operating temperature of the sensor. The structure of the sensor is shown in Fig. 1. The gas-sensing properties of the sensor were measured with a static gas-sensing characterization system, as diagrammed in Fig. 2: sensor was put to the testing chamber from the air chamber, standard NO_2 gas with a certain concentration was injected into the testing chamber in order to get NO_2 gas with ideal concentration. When the resistance reached Rg, the gas is discharged with the help of air intake and exhaust system and electrical fan. The response of the sensor is defined as $S = Rg/Ra$ for oxidizing gas or Ra/Rg for reducing gas, here, Ra and Rg are the resistances of the sensor in the air and target gas, respectively. The response time and recovery time are defined as the time taken by the sensor to achieve 90% of the total resistance change during the adsorption and desorption process, respectively.

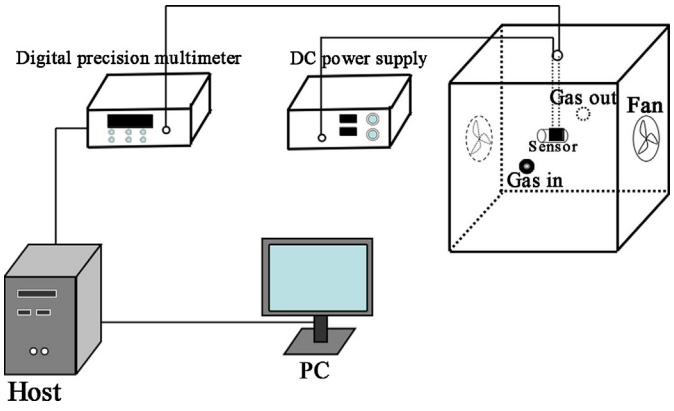

Fig. 2. Testing schematic diagram.

The crystal phase and morphologies of the acid-treated products and calcined products were observed by X-ray powder diffraction (XRD, Rigaku D/max-2550) with Cu Kα1 radiation (λ = 0.15406 nm) at 50 kV/200 mA and the scanning speed was 12° per minute, field emission scanning electron microscopy (SEM, JEOL JSM-7500F, 15 kV), high resolution transmission electron microscopy (HRTEM, JEM 2100F, 200 kV), and selected area electron diffraction (SAED). Thermogravimetric (TG) analysis and differential scanning calorimetric (DSC) measurements were also carried out using a NETZSCH STA 449F3 simultaneous thermogravimetric analyzer under air atmosphere in the temperature range from 25 to 800 °C with a heating rate of 10 °C min^{-1}.

3. Results and discussion

3.1. Structural and morphological characteristics of the prepared WO_3

The XRD patterns of the precursor are given in Fig. S1. The diffraction peaks could not be well indexed to a known substance (not shown here). Fig. 3 shows the XRD patterns of acid-treated product and the sample obtained by calcining acid-treated product at 500 °C. It can be seen that before calcination (Fig. 3b), all the diffraction peaks could be indexed to $H_2W_4O_{13}$ (JCPDS file no.1-583). No peaks of other impurity phases are detected from this pattern. And after calcining at 500 °C, $H_2W_4O_{13}$ was converted into pure monoclinic structure of WO_3 according to JCPDS card No. 89-4480. No characteristic peaks from any other impurities can be observed, indicating that no impurity exists and the $H_2W_4O_{13}$ has completely transformed into the monoclinic WO_3 phase after calcining.

The morphologies and microstructures of the acid-treated and calcined products were illustrated by FESEM observations. Fig. 4a and b shows the detailed morphology of the acid-treated sample, from which 3D flower-like nanostructures with fine nanosheet building units are clearly observed. The average diameter of the

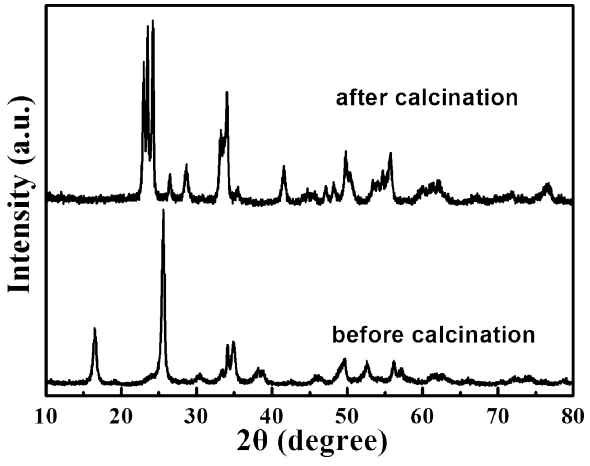

Fig. 3. X-ray diffraction patterns of the as-prepared samples before and after calcining.

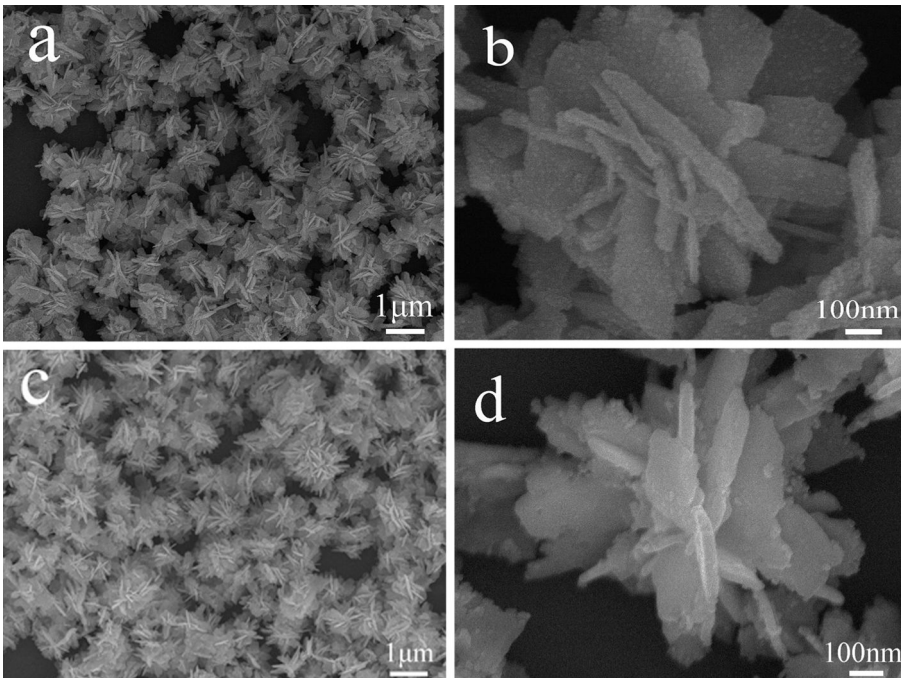

Fig. 4. Morphological characterization of as-synthesized samples: (a) and (b) SEM image of the acid-treated products, (c) and (d) SEM image of the calcined products.

flower-like nanostructures is about 1 μm. Fig. 4b exhibits a high magnification SEM image of the acid-treated sample, demonstrating that dozens of 2D nanosheets with a thickness of about 70 nm are intercrossed with each other and assembled into hierarchical flower-like microstructure. On the basis of the above results, the as-synthesized flower-like structure can be generally classified as hierarchical structures. From the SEM images shown in Fig. 4c and d, the hierarchical nanostructures are maintained after calcining at 500 °C for 2 h. Sintering treatment only induces $H_2W_4O_{13}$ into WO_3 without collapse of the structure. Moreover, the size of each micro-flower diminishes slightly as shown in the high magnification SEM image (Fig. 4d). This might be attributed to the release of water from the thermal decomposition of $H_2W_4O_{13}$.

The constituent nano-units of the flower-like WO_3 obtained after calcining were further investigated by transmission electron microscopy (TEM). The observation of the abundant flower-like nanostructure in Fig. 5a indicates the high yield of the morphology. As can be seen that the size and shape of the product are uniform, which is in agreement with the SEM observation. An individual microflower is given in Fig. 5b, which clearly indicates that the flower-like nanostructure is assembled by loose-packed nanosheets. Fig. 5c is the corresponding HRTEM image taken from a random nanosheet on the flower-like hierarchical WO_3. The space between adjacent lattice planes along a certain direction is 0.387 nm, which is found to correspond to (0 0 2) plane of monoclinic WO_3 crystal (JCPDS No. 89-4480). The selected area electron

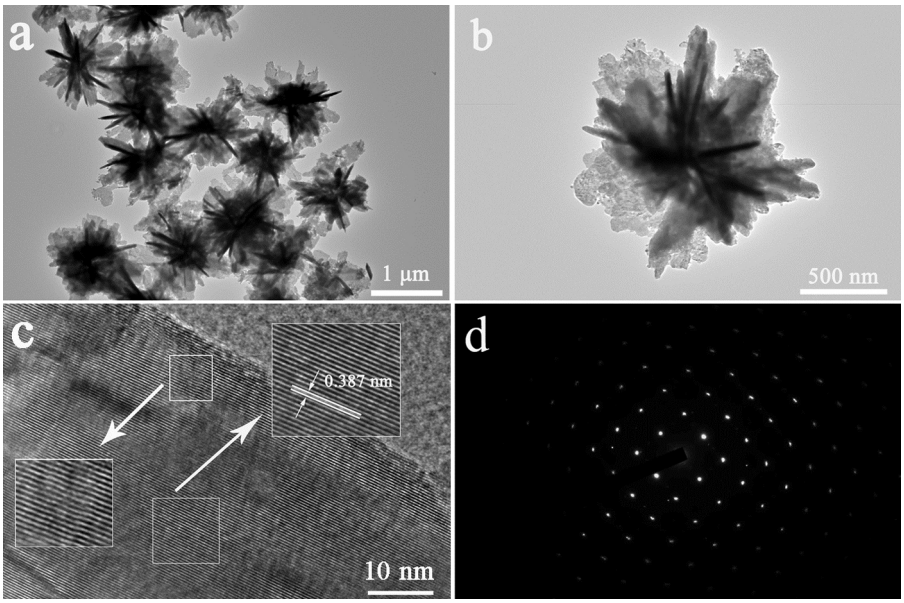

Fig. 5. (a) Typical TEM image of the as-prepared hierarchical flower-like WO_3, (b) the image of an individual flower-like structure, (c) HRTEM image of a nanosheet of the flower, (d) the SAED pattern of an individual WO_3 nanosheet.

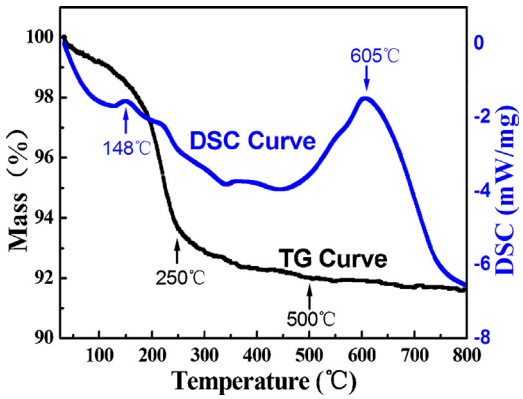

Fig. 6. TG and DSC curves of the acid-treated products.

diffraction (SAED) pattern is shown in Fig. 5d, further confirming that the WO_3 nanosheets are single crystalline in nature.

It is well known that the conversion from $H_2W_4O_{13}$ to WO_3 is realized by release of H_2O after calcining at high temperature. The weight loss was confirmed by Thermogravimetric (TG) and differential scanning calorimetric (DSC) analysis. The curves are displayed in Fig. 6. As shown on the TG curve, the first weight loss (~6.5%) appears between 25 °C and 250 °C (endothermic DSC peak at 148 °C). Here, the slope of the TG curve is very steep. The first weight loss could be attributed to the removal of the water weakly adsorbed to the surface of $H_2W_4O_{13}$. The second weight loss, of 2% occurring between 250 and 500 °C, might be assigned to the release of the water from the thermal decomposition of $H_2W_4O_{13}$, and the combustion of the organics adsorbed on the surface of the sample. After 500 °C, the weight loss does not change significantly, which indicates that the $H_2W_4O_{13}$ is almost entirely converted into WO_3, and the weight tends to be stable. After being oxidized to tungsten trioxide thoroughly (over 500 °C), the crystal will continue to grow in order to lower the surface energy. At the same time, the crystallization of the crystal will improve gradually, corresponding to the exothermic process between 500 and 800 °C of the DSC curve.

To reveal the growth process of flower-like WO_3 and possible growth mechanism, the study of the morphology evolution of flower-like WO_3 nanostructures was conducted with different acidification time. The corresponding results are shown in Fig. 7. When the acidification time was 1 h, only some colloidal nanoparticles could be observed (Fig. 7a). When the acidification time was 6 h, the product was entirely comprised of a relatively uniform aggregates (Fig. 7b). Prolonging the acidification time to 12 h, the flower-like nanostructure became more and more obvious, and the size of the micro-flowers became even more uniform (Fig. 7c). As the reaction time was extended to 21 h, fully developed flower-like architectures were observed (Fig. 7d).

Based on the above experimental results, the growth mechanism of the hierarchical WO_3 nanostructures is tentatively proposed. We consider that the evolution of morphology can be explained by Ostwald ripening mechanism and self assembly process. In the early stage, the nuclei were generated and grew into nanoparticles. In order to minimize the total surface energy, these nanoparticles further aggregated into sphere-like structure with protuberances via the mechanism of Ostwald ripening [31,32]. According to the rule of crystal growth, the secondary nucleation occurs preferentially at sites with more defects as these sites could provide high energy for the growth of nanocrystals [32,33]. Therefore, the dissolving nanoparticles spontaneously nucleated onto these protuberances through an oriented attachment. Due to this anisotropic growth of the crystallized particles along the 2D direction, numerous nanosheets formed gradually. With the consuming of the reactants, these nanosheets assembled into 3D hierarchical microflowers at last.

In order to investigate the gas sensing property, sensor based on the final calcined samples was fabricated. As we all know that the operating temperature has a great influence on the response of a gas sensor based on oxide semiconductor materials [34]. So the optimum temperature of the sensor is first studied here. The responses of the sensor to 40 ppb NO_2 are measured at different temperatures, as shown in Fig. 8. From 50 °C to 90 °C, the response increases with a raise of operating temperature and reaches the maximum value of 96 at 90 °C. When the temperature is further

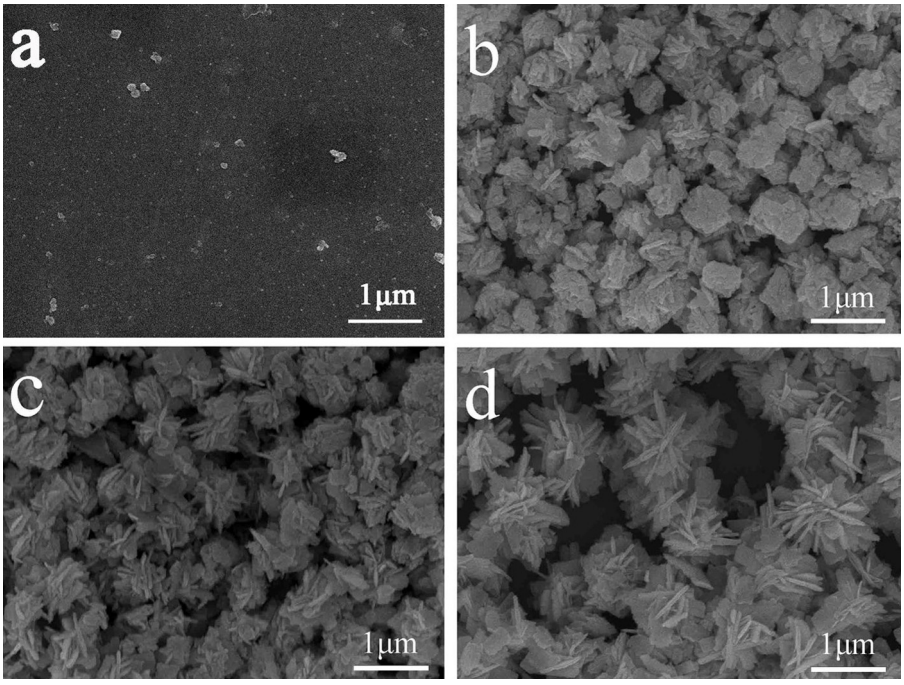

Fig. 7. SEM images of the products obtained at different acid-treated time: (a) 1 h, (b) 6 h, (c) 12 h, (d) 21 h.

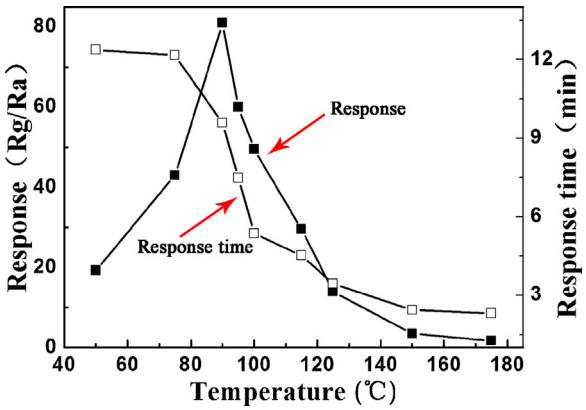

Fig. 8. Response of the sensor to 40 ppb NO_2 as a function of operating temperature.

increased, the response decreases gradually, and it is only about 1.66 at 175 °C, indicating that the response is greatly influenced by working temperature. This phenomenon could be explained as follows: when the temperature is too high, larger amount of oxygen molecules dissociate and adsorb on the active sites, resulting in the decrease of the free active sites for the adsorption of NO_2. On the other hand, the rate of adsorption is lower than desorption at such higher temperature [31,35,36]. Therefore, 90 °C is chosen for the optimum working temperature, which is applied in all the investigations hereinafter.

The response transient curve of the sensor to different concentrations of NO_2 from 0 to 80 ppb at optimum operating temperature is shown in Fig. 9a. The resistance increases when exposed to the gradually increased NO_2 concentration. Namely, the response increases with the increasing of NO_2 concentration. It is interesting to note that the response of the sensor was about 12.8 to 2 ppb of NO_2, indicating that the sensor based on the flower-like WO_3 synthesized here exhibits high response to low concentration of NO_2. The sensing performance between our sensor fabricated here and the literature are compared and shown in Table 1. The results demonstrate that the sensor here has a quite high response to NO_2 and a relative low working temperature.

As is known that the change in resistance is mainly caused by the chemical adsorption and reaction of gas molecules on the surface of the sensing material [37]. In air ambient, oxygen molecules are adsorbed onto the surface of the as-synthesized WO_3 and generate the chemisorbed oxygen species (O_2^-, O^- and O^{2-}) by capturing electrons from the conduction band of WO_3, depletion region is formed on the surface area of WO_3 nanosheets [19]. WO_3 is a kind of n-type oxide semiconductor material with electrons as the major charge carriers and NO_2 is an oxidation gas. Upon exposure to an oxidizing gas (NO_2), gas molecules can easily adsorb on their active sites in the form of NO_2^- ($NO_{2(g)} + e^- \rightarrow NO_2^-{}_{(ads)}$) [35]. Such adsorption and reaction can capture the electrons from WO_3, the thickness of the depletion layer will increase and the carrier concentration decreases. In other words, the resistance of WO_3 will increase when exposed to NO_2.

The reasons for the high response of the sensor to NO_2 are proposed here. One is their unique hierarchical structures of WO_3 assembled by the nanosheets, which offer abundant active sites on the surface and provide favorable conditions for the adsorption of NO_2. It can be observed that the flower-like microstructures are very loose. When the WO_3 are exposed to NO_2 gas, the gas can easily spread inward the sensing body, which is beneficial to enhance the diffusion of NO_2, further induces a higher response. Hence, the unique flower-like microstructure assembled by nanosheets is an important factor to the gas sensing property. On the other hand, a large amount of surface defects can be seen on the single crystal

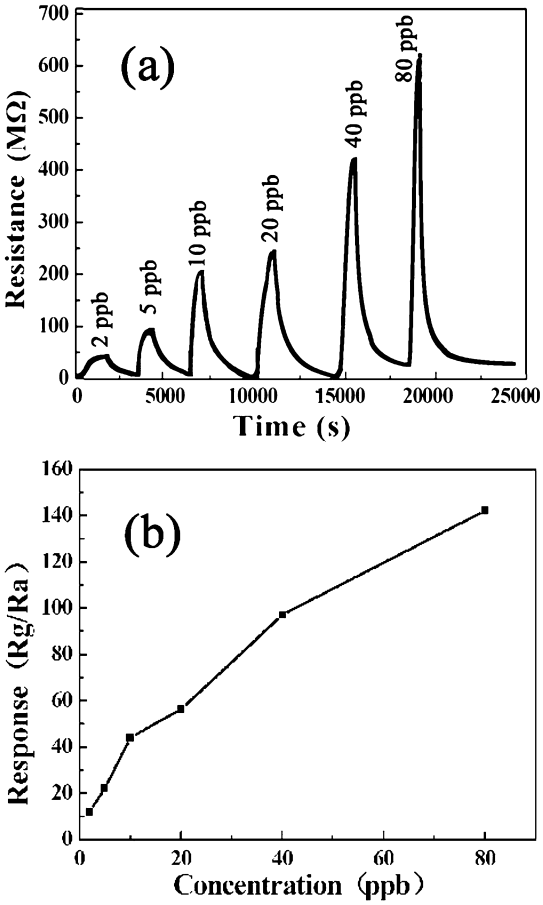

Fig. 9. (a) Response transients of the sensor to different NO_2 concentration at 90 °C. (b) Gas response of the sensor as a function of NO_2 concentrations.

nanosheet (Fig. 5c), making the adsorption and reaction of NO_2 easier. We believe that these reasons are the dominating parameters to cause the high response to NO_2 for the nanosheets assembled microflower. The more detailed reason and qualitative explanation need further investigation.

The selectivity is also the pursuit for a sensor in the view of practical application. Based on this purpose, various gases including oxidizing gases (Cl_2), and reducing gases (CO, H_2S, NH_3, acetone, ethanol) were tested at the optimum working temperature, as shown in Fig. 10. It can be obviously seen that the sensor based on

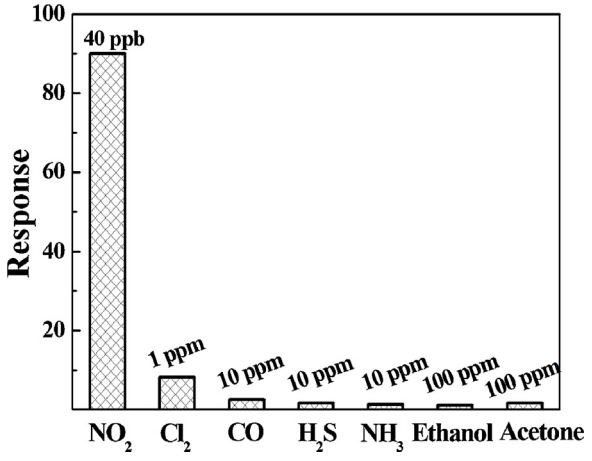

Fig. 10. Comparison of responses of the sensor based on WO_3 to various gases at 90 °C.

Table 1
Gas responses to NO_2 in the present study and those reported in the literatures [14,38–40].

Material	Preparation	NO_2 concentration	Operating temperature	Response	Reference
WO_3	Acid treated	80 ppb	90 °C	152	Present study
WO_3	Acidification	100 ppb	200 °C	40	[38]
WO_3	Hydrothermal	100 ppb	125 °C	92	[14]
WO_3	Sol–gel	100 ppb	300 °C	2	[39]
WO_3	Thermal evaporation	100 ppb	100 °C	18.2	[40]

the flower-like microstructure WO_3 has a larger response to NO_2 compared to the other gases with a high concentration. The results indicate that the sensor has a rather good selectivity to NO_2.

4. Conclusion

In summary, the flower-like WO_3 nanostructures assembled by a number of nanosheets have been successfully synthesized by an acidification method combined with a subsequent annealing process. The characterization results demonstrate that the WO_3 microflowers are composed of numerous nanosheets. The assembled nanosheets are single crystal with ragged edges. In addition, the sensing performance of the sensor based on the as-obtained WO_3 was investigated. The sensor fabricated from these hierarchical structures exhibits excellent sensing properties to NO_2 at relative low operating temperature. The sensor response is about 12.8 to 2 ppb NO_2 at 90 °C. These results suggest that our sensors might have potential application to fabricate highly sensitive and low power consumption NO_2 gas sensor devices.

Acknowledgments

This work is supported by Application and Basic Research of Jilin Province (20130102010JC), the National Nature Science Foundation of China (No. 61304242, 61327804, 61134010, 61377058 and 61374218), Program for Chang Jiang Scholars and Innovative Research Team in University (No. IRT13018) and “863” High Technology Project (2013AA030902 and 2014AA06A505).

Appendix A. Supplementary data

Supplementary data associated with this article can be found, in the online version, at http://dx.doi.org/10.1016/j.snb.2014.07.083.

References

[1] J.Y. Lao, J.Y. Huang, D.Z. Wang, Z.F. Ren, Hierarchical oxide nanostructures, J. Mater. Chem. 14 (2004) 770–773.
[2] L. Vayssieres, Growth of arrayed Nanorods and nanowires of ZnO from aqueous solutions, Adv. Mater. 15 (2003) 464–466.
[3] C.W. Cheng, B. Liu, H.Y. Yang, W.W. Zhou, L. Sun, R. Chen, S.F. Yu, H. Gong, J.X. Zhang, H.D. Sun, H.J. Fan, Hierarchical assembly of ZnO nanostructures on SnO_2 backbone nanowires: low temperature hydrothermal preparation and optical properties, ACS Nano 3 (2009) 3069–3076.
[4] X.W. Lou, Y. Wang, C. Yuan, J.Y. Lee, L.A. Archer, Template-free synthesis of SnO_2 hollow nanostructures with high lithium storage capacity, Adv. Mater. 18 (2006) 2325–2329.
[5] Y.L. Wang, X.C. Jiang, Y.N. Xia, A solution-phase, precursor route to polycrystalline SnO_2 nanowires that can be used for gas sensing under ambient conditions, J. Am. Chem. Soc. 125 (2003) 16176–16177.
[6] X.C. Jiang, T. Herricks, Y.N. Xia, CuO nanowires can be synthesized by heating copper substrates in air, Nano Lett. 12 (2002) 1333–1338.
[7] B. Liu, H.C. Zeng, Mesoscale organization of CuO nanoribbons: formation of dandelions, J. Am. Chem. Soc. 126 (2004) 8124–8125.
[8] D.H. Zhang, Z.Q. Liu, C. Li, T. Tang, X.L. Liu, S. Han, B. Lei, C.W. Zhou, Detection of NO_2 down to ppb levels using individual and multiple In_2O_3 nanowire devices, Nano Lett. 4 (2004) 1919–1924.
[9] C. Li, D. Zhang, S. Han, X. Liu, T. Tang, C. Zhou, Diameter-controlled growth of single-crystalline In_2O_3 nanowires and their electronic properties, Adv. Mater. 15 (2003) 143–146.
[10] S.J. Bao, C.M. Li, J.F. Zang, X.Q. Cui, Y. Qiao, J. Guo, New nanostructured TiO_2 for direct electrochemistry and glucose sensor applications, Adv. Funct. Mater. 18 (2008) 591–599.
[11] C.W. Cheng, S.K. Karuturi, L.J. Liu, J.P. Liu, H.X. Li, L.T. Su, A.I.Y. Tok, H.J. Fan, Quantum dots sensitized TiO_2 inverse opal for photoelectrochemical hydrogen generation, Small 8 (2012) 37–42.
[12] W.J. Li, Z.W. Fu, Nanostructured WO_3 thin film as a new anode material for lithium-ion batteries, Appl. Surf. Sci. 256 (2010) 2447–2452.
[13] C. Santato, M. Ulmann, J. Augustynski, Photoelectrochemical properties of nanostructured tungsten trioxide films, J. Phys. Chem. B 105 (2001) 936–940.
[14] L. You, Y.F. Sun, J. Ma, Y. Guan, J.M. Sun, Y. Du, G.Y. Lu, Highly sensitive NO_2 sensor based on square-like tungsten oxide prepared with hydrothermal treatment, Sens. Actuators B: Chem. 157 (2011) 401–407.
[15] B.P. Jelle, G. Hagen, Performance of an electrochromic window based on polyaniline prussian blue and tungsten oxide, Sol. Energy Mater. Sol. Cells 58 (1999) 277–286.
[16] C. Cantalini, H.T. Sun, M. Faccio, M. Pelino, S. Santucci, L. Lozzi, M. Passacantando, NO_2 sensitivity of WO_3 thin film obtained by high vacuum thermal evaporation, Sens. Actuators B: Chem. 31 (1996) 81–87.
[17] H. Baeck1, K.S. Choi, T.F. Jaramillo1, G.D. Stucky, E.W. McFarl, Enhancement of photocatalytic and electrochromic properties of electrochemically fabricated mesoporous WO_3 thin films, Adv. Mater. 15 (2003) 1269–1273.
[18] K. Galatsis, Y.X. Lia, W. Wlodarski, K. Kalantarzadeh, Sol–gel prepared MoO_3-WO_3 thin-films for O_2 gas sensing, Sens. Actuators B: Chem. 77 (2001) 478–483.
[19] N. Yamazoe, G. Sakai, K. Shimanoe, Oxide semiconductor gas sensors, Catal. Surv. Asi. 7 (2003) 63–75.
[20] X.H. Xia, J.P. Tu, J. Zhang, X.L. Wang, W.K. Zhang, H. Huang, Morphology effect on the electrochromic and electrochemical performances of NiO thin films, Electrochim. Acta 53 (2008) 5721–5724.
[21] J. Silver, M.I. Martinez-Rubio, T.G. Ireland, G.R. Fern, R. Withnall, The effect of particle morphology and crystallite size on the upconversion luminescence properties of erbium and ytterbium Co-doped yttrium oxide phosphors, J. Phys. Chem. B 105 (2001) 948–953.
[22] S.D. Oosterhout1, M.M. Wienk1, S.S. Bavel, R. Thiedmann, L. Jan Anton Koster, J. Gilot, J. Loos, V. Schmidt, R.A.J. Janssen, The effect of three-dimensional morphology on the efficiency of hybrid polymer solar cells, Nanostruct. Mater. 8 (2009) 818–824.
[23] Y.M. Zhao, Y.Q. Zhu, Room temperature ammonia sensing properties of $W_{18}O_{49}$ nanowires, Sens. Actuators B: Chem. 137 (2009) 27–31.
[24] Y. Lu, Y.F. Sun, Y. Guan, J.M. Sun, Y. Du, G.Y. Lu, Highly sensitive NO_2 sensor based on square-like tungsten oxide prepared with hydrothermal treatment, Sens. Actuators B: Chem. 157 (2011) 401–407.
[25] C.Y. Lee, S.J. Kim, I.S. Hwang, J.H. Lee, Glucose-mediated hydrothermal synthesis and gas sensing characteristics of WO_3 hollow microspheres, Sens. Actuators B: Chem. 142 (2009) 236–242.
[26] G. Xi, J. Ye, Q. Ma, N. Su, H. Bai, C. Wang, In situ growth of metal particles on 3D urchin-like WO_3 nanostructures, J. Am. Chem. Soc. 134 (2012) 6508–6511.
[27] C. Ng, C. Ye, Y.H. Ng, R. Amal, Flower-shaped tungsten oxide with inorganic fullerene-like structure: synthesis and characterization, Cryst. Growth Des. 10 (2010) 3794–3801.
[28] Y. Zhao, H. Chen, X. Wang, J. He, Y. Yu, H. He, Flower-like tungsten oxide particles: synthesis, characterization and dimethyl methylphosphonate sensing properties, Anal. Chim. Acta 675 (2010) 36–41.
[29] S. Sen, A. Vitae, P. Kanitkar, A. Sharma, K.P. Muthe, A. Rath, S.K. Deshpande, M. Kaur, R.C. Aiyer, S.K. Gupta, J.V. Yakhmi, Growth of SnO_2/$W_{18}O_{49}$ nanowire hierarchical heterostructure and their application as chemical sensor, Sens. Actuators B: Chem. 147 (2010) 453–460.
[30] X. Shen, G. Wang, D. Wexler, Large-scale synthesis and gas sensing application of vertically aligned and double-sided tungsten oxide nanorod arrays, Sens. Actuators B: Chem. 143 (2009) 325–332.
[31] X.Q. An, J.C. Yu, Y. Wang, Y.M. Hu, X.L. Yu, G.J. Zhang, WO_3 nanorods/graphene nanocomposites for high-efficiency visible-light-driven photocatalysis and NO_2 gas sensing, J. Mater. Chem. 22 (2012) 8525–8531.
[32] T.L. Sounart, J. Liu, J.A. Voigt, M. Huo, E.D. Spoerke, B.M. Kenzie, Secondary nucleation and growth of ZnO, J. Am. Chem. Soc. 129 (2007) 15786–15793.
[33] G.C. Xi, K. Xiong, Q.B. Zhao, R. Zhang, H.B. Zhang, Y.T. Qian, Nucleation-dissolution-recrystallization: a new growth mechanism fort-selenium nanotubes, Cryst. Growth Des. 6 (2006) 577–582.
[34] Z. Cao, J.R. Stetter, A selective solid-state gas sensor for halogenated hydrocarbons, Sens. Actuators B: Chem. 5 (1991) 109–113.
[35] B. Ruhland, Th. Becker, G. Müller, Gas-kinetic interactions of nitrous oxides with SnO2 surface, Sens. Actuators B: Chem. 50 (1998) 85–94.

[36] A.P. Lee, B.J. Reedy, Temperature modulation in semiconductor gas sensing, Sens. Actuators B: Chem. 60 (1999) 35–42.
[37] N. Yamazoe, New approaches for improving semiconductor gas sensors, Sens. Actuators B: Chem. 5 (1991) 7–19.
[38] T. Kida, A. Nishiyama, M. Yuasa, K. Shimanoe, N. Yamazoe, Highly sensitive NO_2 sensors using lamellar-structured WO_3 particles prepared by an acidification method, Sens. Actuators B: Chem. 135 (2009) 568–574.
[39] S.Han. Wang, T.C. Choua, C.C. Liu, Nano-crystalline tungsten oxide NO_2 sensor, Sens. Actuators B: Chem. 94 (2003) 343–351.
[40] A. Ponzoni, E. Comini, M. Ferroni, G. Sberveglieri, Nanostructured WO_3 deposited by modified thermal evaporation for gas-sensing applications, Thin Solid Films 490 (2005) 81–85.

Biographies

Chong Wang received the B. Eng. degree in department of electronic sciences and technology in 2013. Now he is currently studying for his M.E. Sci. degree in College of Electronic Science and Engineering, Jilin University, China.

Ruize Sun received the B. Eng. degree in department of electronic sciences and technology in 2012. Now he is currently studying for his M.E. Sci. degree in College of Electronic Science and Engineering, Jilin University, China.

Xin Li received the B. Eng. degree in department of electronic sciences and technology in 2013. Now he is currently studying for his M.E. Sci. degree in College of Electronic Science and Engineering, Jilin University, China.

Yanfeng Sun obtained his Ph.D. from Jilin University of China in 2007. Presently, he is working as associate professor in Electronics Science and Engineering department of Jilin University. His current research interests are nanoscience and gas sensors.

Peng Sun received his MS degree from State Key Laboratory of Superhard Materials, Jilin University, China in 2009. He entered the Ph.D. course in 2010, majored in microelectronics and solid-state electronics. Now, he is engaged in the synthesis and characterization of the semiconducting functional materials and gas sensors.

Fengmin Liu received the BE degree in Department of Electronic Science and Technology in 2000. She received his Doctor's degree in College of Electronic Science and Engineering at Jilin University in 2005. Now she is a professor in Jilin University, China. Her current research is preparation and application of semiconductor oxide, especial in gas sensor and solar cell.

Geyu Lu received the BS degree in electronic sciences in 1985 and the MS degree in 1988 from Jilin University in China and the Dr Eng degree in 1998 from Kyushu University in Japan. Now he is a professor of Jilin University, China. Now, he is interested in the development of functional materials and chemical sensors.